

Intermittent jet activity in the radio galaxy 4C29.30?

M. Jamrozy¹*, C. Konar², D.J. Saikia², Ł. Stawarz^{1,3,4}, K.-H. Mack⁵, A. Siemiginowska⁶

¹ *Obserwatorium Astronomiczne, Uniwersytet Jagielloński, ul. Orła 171, PL-30244 Kraków, Poland*

² *National Centre for Radio Astrophysics, TIFR, Pune University Campus, Post Bag 3, Pune 411 007, India*

³ *Kavli Institute for Particle Astrophysics and Cosmology, Stanford University, Stanford CA 94305, USA*

⁴ *Stanford Linear Accelerator Center, Menlo Park CA 94025, USA*

⁵ *Istituto Nazionale di Astrofisica, Istituto di Radioastronomia, Via P. Gobetti 101, I-40129 Bologna, Italy*

⁶ *Harvard-Smithsonian Center for Astrophysics, 60 Garden Street, Cambridge, MA 02138, USA*

Accepted. Received

ABSTRACT

We present radio observations at frequencies ranging from 240 to 8460 MHz of the radio galaxy 4C29.30 (J0840+2949) using the Giant Metrewave Radio Telescope (GMRT), the Very Large Array (VLA) and the Effelsberg telescope. We report the existence of weak extended emission with an angular size of \sim 520 arcsec (639 kpc) within which a compact edge-brightened double-lobed source with a size of 29 arcsec (36 kpc) is embedded. We determine the spectrum of the inner double from 240 to 8460 MHz and show that it has a single power-law spectrum with a spectral index is \sim 0.8. Its spectral age is estimated to be \lesssim 33 Myr. The extended diffuse emission has a steep spectrum with a spectral index of \sim 1.3 and a break frequency \lesssim 240 MHz. The spectral age is \gtrsim 200 Myr, suggesting that the extended diffuse emission is due to an earlier cycle of activity. We reanalyse archival x-ray data from Chandra and suggest that the x-ray emission from the hotspots consists of a mixture of nonthermal and thermal components, the latter being possibly due to gas which is shock heated by the jets from the host galaxy.

Key words: galaxies: active – galaxies: nuclei – galaxies: individual: 4C29.30 – radio continuum: galaxies

1 INTRODUCTION

One of the interesting issues in our understanding of active galactic nuclei (AGN) is the duration of their active phase and whether such activity is episodic. In radio galaxies and quasars the extended radio emission provides us with an opportunity to probe their history via the structural and spectral information of the lobes. A striking example of episodic nuclear activity is when a new pair of radio lobes is seen closer to the nucleus before the ‘old’ and more distant radio lobes have faded (e.g. Subrahmanyan, Saripalli & Hunstead 1996; Lara et al. 1999). Such sources have been christened as ‘double-double’ radio galaxies (DDRGs) by Schoenmakers et al. (2000). Approximately a dozen or so of such DDRGs are known in the literature (Saikia, Konar & Kulkarni 2006, and references therein).

In addition, diffuse relic radio emission due to an earlier cycle of activity may also be visible around radio sources

which are not characterised by a ‘classical double’ structure with hotspots at the outer edges. The relic radio emission is expected to remain visible for \sim 10⁸ yr or so (e.g. Owen, Eilek & Kassim 2000; Kaiser & Cotter 2002; Jamrozy et al. 2004), and have a steep radio spectrum due to radiative losses. Such radio emission possibly due to an earlier cycle of activity has been suggested for a number of sources from both structural and spectral information. These include 3C338 and 3C388 (Burns, Schwendeman & White 1983; Roettiger et al. 1994), Her A (Gizani & Leahy 2003), 3C310 (van Breugel & Fomalont 1984; Leahy et al. 1986), and Cen A (Burns, Feigelson & Schreier 1983; Clarke, Burns & Norman 1992; Junkes et al. 1993; Morganti et al. 1999). There have also been a few candidates amongst compact radio sources. For example, a lobe of emission seen on one side of the nuclear region in the Giga-hertz Peaked Spectrum (GPS) source B0108+388 has been suggested to be a relic of a previous cycle of jet activity (Baum et al. 1990), although the one-sidedness of the emission is puzzling (cf. Stanghellini et al. 2005). A search for small-scale halos, on scales larger than the known milliarcsec-scale structures of compact steep spectrum and GPS sources, using interplanetary scintillation observations

* E-mail: jamrozy@oa.uj.edu.pl (MJ); sckonar@ncra.tifr.res.in (CK); djs@ncra.tifr.res.in (DJS); stawarz@oa.uj.edu.pl (LS); mack@ira.inaf.it (KHM); asiemiginowska@cfa.harvard.edu (AS)

with the Ooty Radio Telescope at 327 MHz led to the identification of a few possible candidates (Jeyakumar et al. 2000). However, such features are not very common in either small or large radio sources. For example, a number of searches for such features have not yielded clear and striking examples of relic emission around bright radio sources (e.g. Reich et al. 1980; Stute, Reich & Kalberla 1980; Perley, Fomalont & Johnston 1982; Kronberg & Reich 1983; van der Laan, Zieba & Noordam 1984; Jones & Preston 2001).

In this paper we concentrate on the radio galaxy 4C29.30 (J0840+2949) which is associated with a bright ($R \sim 15^m$) host elliptical galaxy (RA $08^h40^m02\rlap{.}^s370$, DEC $+29^\circ49'02\rlap{.}''60$; all positions being in J2000 co-ordinates throughout the paper) at a redshift of 0.06471 ± 0.00013 . The corresponding luminosity distance is 287 Mpc and 1 arcsec corresponds to 1.228 kpc in a Universe with $H_0=71 \text{ km s}^{-1} \text{ Mpc}^{-1}$, $\Omega_m=0.27$, $\Omega_\Lambda=0.73$ (Spergel et al. 2003). The published images show a double-lobed radio source which has two prominent hotspots at the outer edges with an overall angular separation of 29 arcsec (36 kpc) and a prominent jet towards the south-west (e.g. van Breugel et al. 1986; Parma et al. 1986 and references therein). In addition there is a diffuse blob of emission towards the south-west (SW blob) with a size of ~ 40 arcsec (50 kpc) extending beyond the southwestern hotspot. The radio luminosity of the inner double at 1400 MHz is $5.5 \times 10^{24} \text{ W Hz}^{-1}$, which is significantly below the dividing line of the Fanaroff-Riley classes, while that of the entire source is $7.4 \times 10^{24} \text{ W Hz}^{-1}$. It is interesting to note that in some of the DDRGs, the luminosity of the inner double is in the FRI category although its structure resembles that of FRII radio sources (cf. Saikia et al. 2006). A detailed radio and optical study of this galaxy (van Breugel et al. 1986) shows optical line-emitting gas adjacent to the radio jet along a position angle (PA) of $\sim 20^\circ$ and evidence of the radio jets interacting with dense extranuclear gas.

The host galaxy of 4C29.30 appears to have merged with a gas-rich galaxy, shows presence of shells and dust (Gonzalez-Serrano, Carballo & Perez-Fournon 1993) and is associated with an IRAS source F08369+2959 (Keel et al. 2005). At x-ray wavelengths Chandra detects emission from the hot spots in the southwestern radio lobe and also in the counterlobe (Gambill et al. 2003; Sambruna et al. 2004). Both hotspots have also been detected in observations with the Hubble Space Telescope (Sambruna et al. 2004).

In this paper we show the presence of diffuse extended emission on an angular scale of ~ 520 arcsec (639 kpc) which could be due to an earlier cycle of activity, from observations with the Very Large Array (VLA), the Giant Metrewave Radio Telescope (GMRT) and the Effelsberg telescope. This feature is also visible clearly in the Westerbork Northern Sky Survey (WENSS; Rengelink et al. 1997) at 325 MHz and the NRAO VLA Sky Survey (NVSS; Condon et al. 1998) at 1400 MHz. We also present multifrequency observations of the inner double and the diffuse SW blob of emission with the GMRT and the VLA. This should enable us to determine the spectrum more reliably and estimate the spectral ages and perhaps constrain the time scales of episodic activity in this source. For example, in the DDRG J1453+3308 we have been able to show using both GMRT and VLA observations that the spectrum of the outer lobes exhibits significant curvature while that of the inner lobes appears practically straight (Konar et al. 2006).

Table 1. Observing log.

Telescope	Array Conf.	Obs. Freq. (MHz)	Bandwidth (MHz)	Primary beam (arcmin)	Obs. Date
(1)	(2)	(3)	(4)	(5)	(6)
GMRT		240	4.5	114	2005 Dec 28
GMRT		333	12.5	81	2005 Dec 24
GMRT		605	12.5	43	2005 Dec 28
GMRT		1287	12.5	26	2005 Dec 22
VLA ^a	D	1400	25	30	2001 Nov 30
VLA ^a	D	1400	25	30	2001 Dec 24
VLA ^a	C	4860	50	9	1988 Apr 14
VLA	CnD	4860	50	9	2005 Oct 9, 10
VLA	CnD	8460	50	5.4	2005 Oct 12
Effelsberg		4850	500	2.1	2004 Jun 25

^a: VLA archival data.

Our multifrequency observations and data reduction are described in Section 2. The observational results, such as the radio maps showing the source structure and spectra are presented in Section 3. The results are presented in Section 4, while the concluding remarks are given in Section 5.

2 OBSERVATIONS AND DATA REDUCTION

The analysis presented in this paper is based on radio observations made with the Effelsberg telescope, GMRT and VLA, as well as on VLA archival data. The observing log for both the GMRT and VLA as well as Effelsberg observations is listed in Table 1 which is arranged as follows. Columns 1 and 2 show the name of the telescope, and the array configuration for the VLA observations; columns 3 and 4 show the frequency and bandwidth used in making the images; column 5: the primary beamwidth in arcmin; column 6: dates of the observations. The phase centre for all the observations was near the core of the radio galaxy except for the VLA CnD array observations at 5 GHz where the antennas were pointed about 2 arcmin north and south of the core in an effort to detect the diffuse extended emission.

2.1 GMRT observations

The observations were made in the standard manner, with each observation of the target-source interspersed with observations of 3C286 which was used as a phase calibrator as well as flux density and bandpass calibrator. At each frequency the source was observed in a full-synthesis run of approximately 9 hours including calibration overheads. The rms noise in the resulting full-resolution images ranges from about 1 mJy beam^{-1} at 240 MHz to about $0.06 \text{ mJy beam}^{-1}$ at 1287 MHz. Details about the array can be found at the GMRT website at <http://www.gmrt.ncra.tifr.res.in>. The data collected were calibrated and reduced in the standard way using the NRAO AIPS software package. Several rounds of self calibration were done to improve the quality of the images. The absolute position uncertainty could be up to several arcsec in the low-frequency images due to phase errors introduced by the ionosphere (cf. Rengelink et al. 1997). The flux densities at the different frequencies are consistent with the scale of Baars et al. (1977).

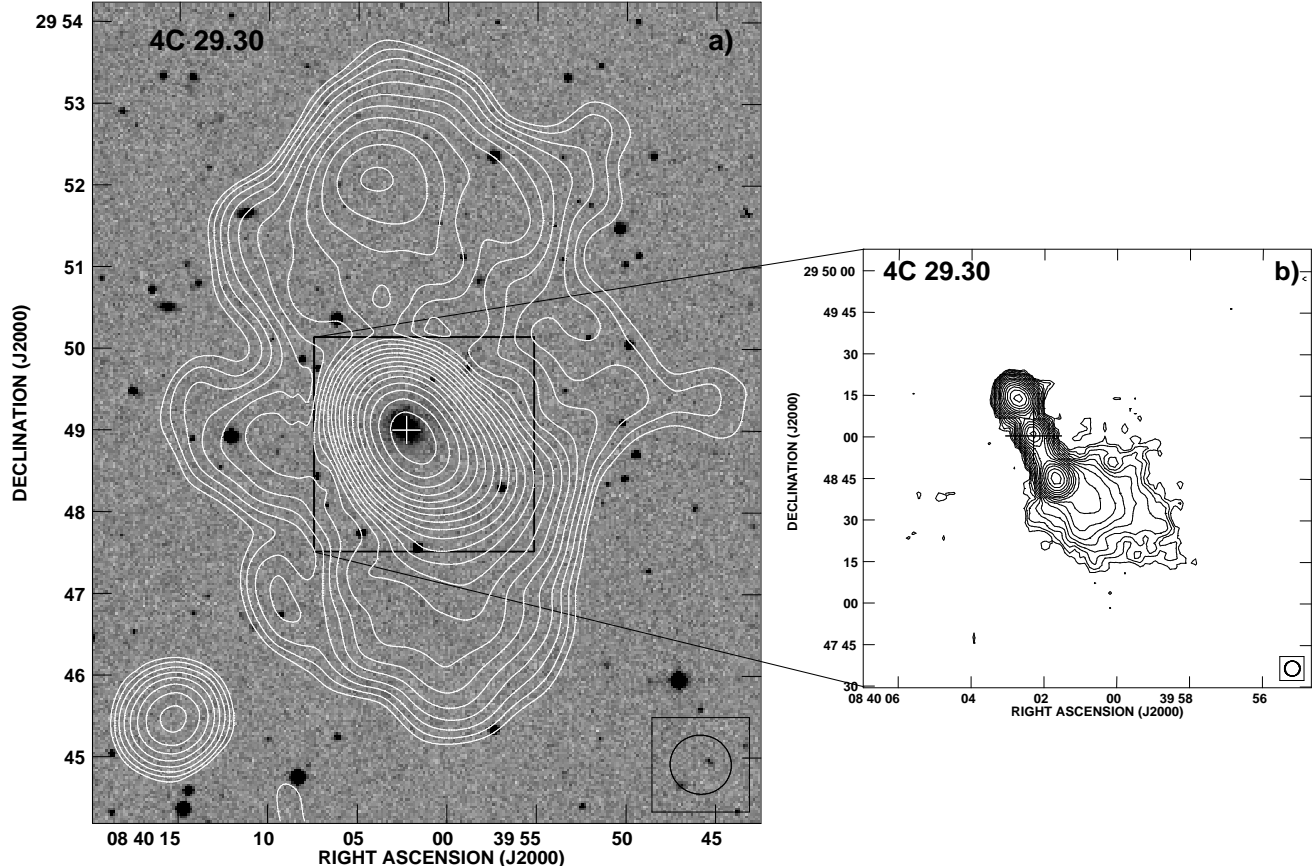


Figure 1. 1400-MHz VLA images of 4C 29.30. **a)** D-array contour map of the entire source overlaid on the optical field from the Digital Sky Survey (DSS). The contour levels are spaced by factors of $\sqrt{2}$ and the first contour is $0.3 \text{ mJy beam}^{-1}$. **b)** B-array contour map of the central part of the source from FIRST. The contour levels are spaced by factors of $\sqrt{2}$, and the first contour is $0.45 \text{ mJy beam}^{-1}$. The size of the beam is indicated by an ellipse in the bottom right corner of each image. The cross marks the position of the radio core.

2.2 New and archival VLA observations

The source was observed with the CnD array at a frequency of 4860 and 8460 MHz to determine the spectra over a large frequency range by combining these results with those from the low-frequency GMRT images. The source was observed in the snapshot mode, the integration time for each scan being ~ 20 min. At 4860 MHz the source was also observed with the phase centres shifted by ~ 2 arcmin towards the north and south of the core to image the diffuse extended emission. The interferometric phases were calibrated with the phase calibrator J0830+241. The source 3C286 was used as the primary flux density calibrator. For the images produced from the data sets where the phase centres have been shifted by ~ 2 arcmin, correction for the primary beam pattern has been done. We also supplemented our observations with VLA archival data to examine evidence of variability of the core and determine the spectrum of the inner double-lobed source. These observations were made with the C-array at 4860 MHz.

We retrieved the L-band data of 4C29.30 from the VLA archive. The unpublished observations (proposal number AL515) were carried out in the D-array configuration using the ‘Correlator Mode 4’ with a bandwidth of 25 MHz and central frequencies of 1365 and 1435 MHz. The observations were performed in two runs on 2001 November 30 and

December 24 with the pointing centre at RA $08^{\text{h}}40^{\text{m}}02^{\text{s}}.3$, DEC $+29^{\circ}49'03''.0$ and a total integration time of 2×50 min. The telescope gains were calibrated using the calibration source 3C147. The source J0741+312 was used as a phase calibrator. After the initial data reduction the two data sets were merged using the task DBCON. After preliminary CLEANing of the map with the routine IMAGR, several self-calibrations were performed to improve its quality. Finally, the map was corrected for primary beam attenuation. As in the case of the GMRT data, all the VLA data were edited and reduced using the AIPS package. All flux densities are on the Baars et al. (1977) scale.

2.3 Effelsberg observations

The 4850-MHz observations of 4C 29.30 were carried out on 2004 June 25 with the 2-horn receiver system (Thierbach, Klein & Wielebinski 2003) at the secondary focus of the Effelsberg 100-m telescope. A total of 6 coverages, with a size of 20×20 arcmin 2 in azimuth and elevation, were obtained. The scanning speed was 40 arcmin/min and the scan separation 1 arcmin. Calibration and pointing performance of the system were checked by mapping and cross-scanning the point-like sources, 3C286 and B0851+20. We adopt the flux density scale of Baars et al. (1977). The standard MPIF-

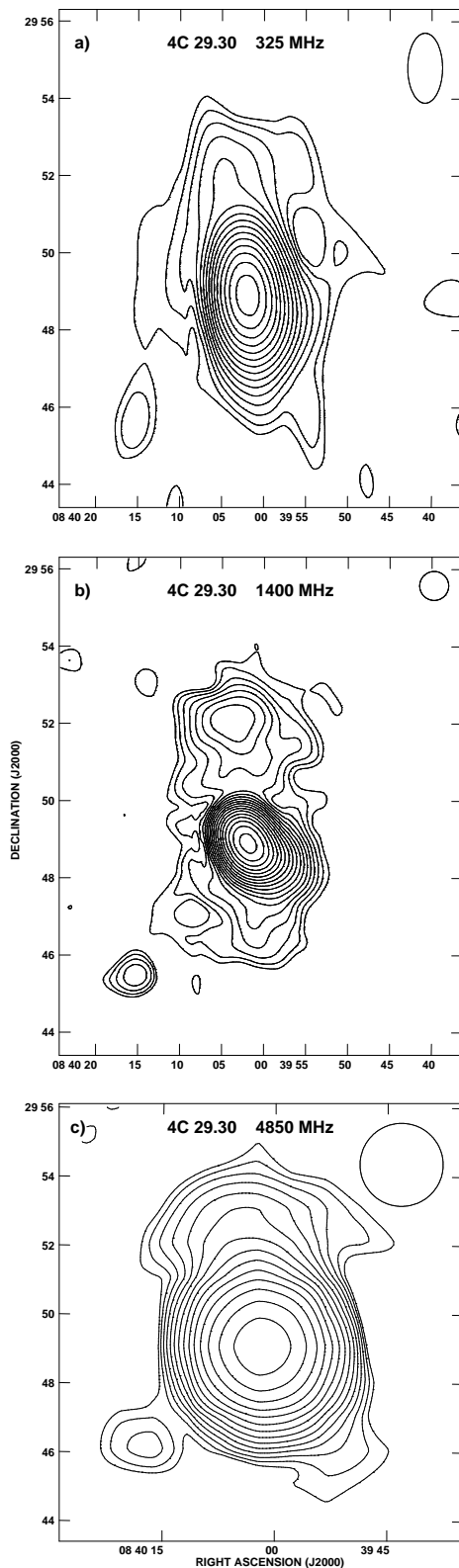


Figure 2. Atlas of the radio source 4C 29.30 at three different radio frequencies. **a)** 325-MHz map from the WENSS, **b)** 1400-MHz map from the NVSS, **c)** 4850-MHz map from the Effelsberg observations. The contours spaced by factors of $\sqrt{2}$ in brightness are plotted starting with 9, 0.9 and 1.8 mJy beam $^{-1}$ respectively. The size of the beam is indicated by an ellipse in the top right corner of each image.

NOD2 (Haslam 1974) software package was used for the data reduction. Firstly, all single-pixel noise spikes were removed by hand from each of the scans. Then the individual maps were combined using the PLAIT algorithm by Emerson & Gräve (1988). The rms noise of 0.9 mJy beam $^{-1}$ in total power was estimated from off-source regions of the image well away from its edges and the half-power beam width was determined to be 144.5 arcsec. Finally, the NRAO AIPS software package was used for imaging the source.

3 OBSERVATIONAL RESULTS

3.1 Overall structure

Our VLA image at 1400 MHz with an angular resolution of ~ 45 arcsec (Fig. 1) shows the entire structure of 4C29.30 which has a largest angular extent of 520 arcsec (639 kpc), in addition to the inner structure with an angular size of 29 arcsec (36 kpc). The rms noise in the image is 0.13 mJy beam $^{-1}$ while the total flux density is 756 mJy. There is a peak of emission with a peak brightness of 10 mJy beam $^{-1}$ located at RA 08 $^{\mathrm{h}} 40^{\mathrm{m}} 04^{\mathrm{s}}.03$, DEC +29 $^{\circ} 52' 04''.4$ in the northern region of the extended emission which is brighter than the south which has a peak brightness of ~ 3.5 mJy beam $^{-1}$ at RA 08 $^{\mathrm{h}} 39^{\mathrm{m}} 59^{\mathrm{s}}.29$, DEC +29 $^{\circ} 46' 32''.3$. We have reproduced in Fig. 1 the FIRST (Faint Images of the Radio Sky at Twenty-cm, Becker, White & Helfand 1995) image of the source with an angular resolution of 5.4 arcsec which shows the inner double-lobed structure and the SW blob of emission. Due to lack of short baselines this VLA B-array survey is insensitive to the extended structures.

The diffuse extended structure can also be seen in our Effelsberg image at 4850 MHz as well as the WENSS image at 325 MHz and the NVSS image at 1400 MHz (Fig. 2). The 325-MHz WENSS map of the total intensity emission of 4C29.30 with the angular resolution of about 54 \times 109 arcsec 2 (Fig. 2a) has an rms noise of 3.9 mJy beam $^{-1}$ while the total flux density of the entire source is 2170 mJy. The total intensity 1400-MHz VLA D-array NVSS map of the source with an angular resolution of 45 \times 45 arcsec 2 and an rms noise of 0.45 mJy beam $^{-1}$ (Fig. 2b) has a total flux density of 731 mJy, which is only marginally smaller than the estimate of 756 mJy from our image (Fig. 1).

Although only the inner double and the SW blob of emission are visible in the full-resolution GMRT images as discussed below, tapered images with an angular resolution of 45 arcsec were made from the GMRT data at 240, 333, 605 and 1287 MHz to detect the diffuse extended emission. These images are presented in Fig. 3 and have an rms noise of 4.6, 1.6, 0.9 and 0.5 mJy beam $^{-1}$ respectively, while the total flux densities are 3541, 2647, 1465 and 727 mJy respectively. A comparison of the GMRT low-resolution images with our VLA D-array image (Fig. 1) shows that although the northern peak and some diffuse emission have been detected, weaker diffuse emission have been missed in these images. While at the lower frequencies this is due to the higher rms noise values, the flux density at 1287 MHz could also be affected by the lack of short spacings.

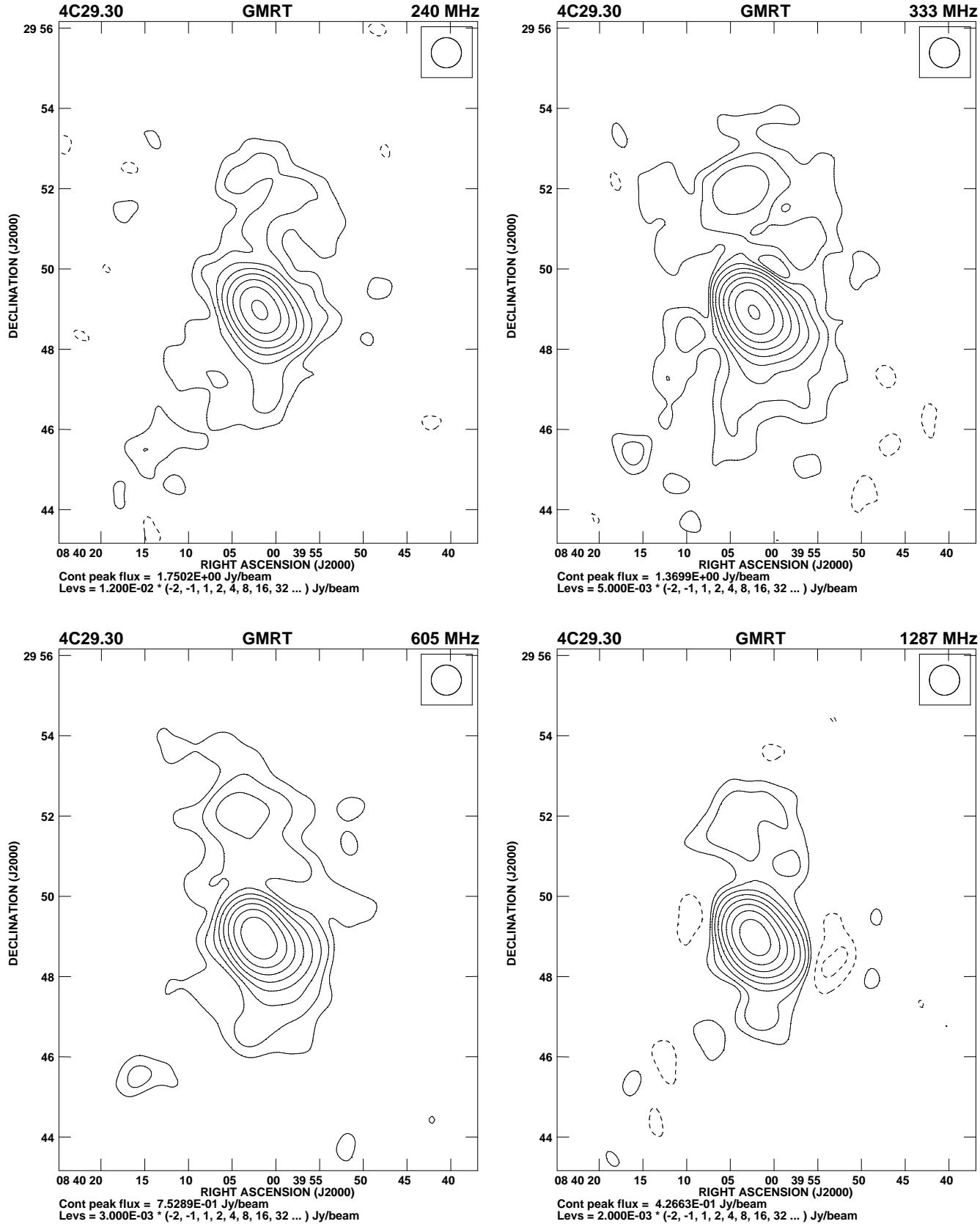


Figure 3. The GMRT images of 4C29.30 at 240 MHz (upper left), 333 MHz (upper right), 605 MHz (lower left) and 1287 MHz (lower right). All these images have been made with an angular resolution of 45 arcsec which is shown as a circle in the top right-hand corner.

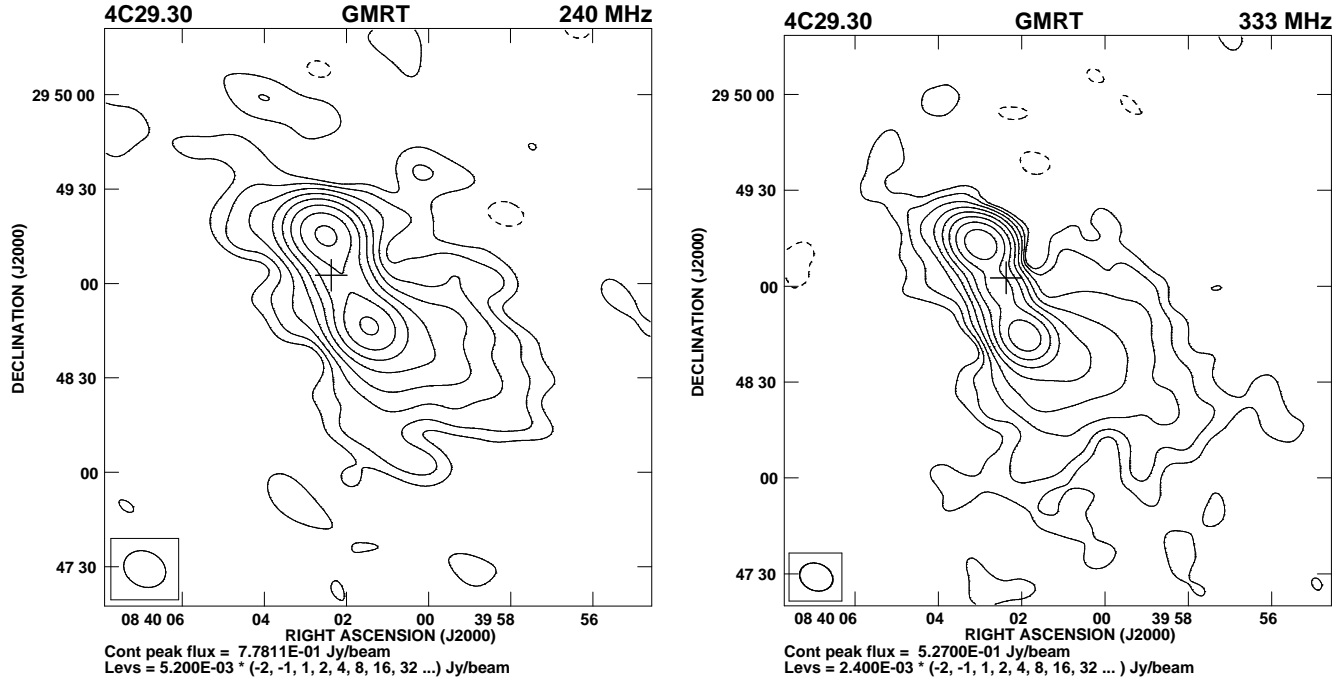


Figure 4. The GMRT images of 4C29.30. Left-hand panel: image at 240 MHz with an angular resolution of 13.8×11.1 arcsec 2 along PA 64 $^\circ$. Right-hand panel: the 333-MHz image with an angular resolution of 10.6×8.5 arcsec 2 along PA 68 $^\circ$. The resolution is shown as an ellipse in the bottom left-hand corner while the + sign marks the position of the optical galaxy.

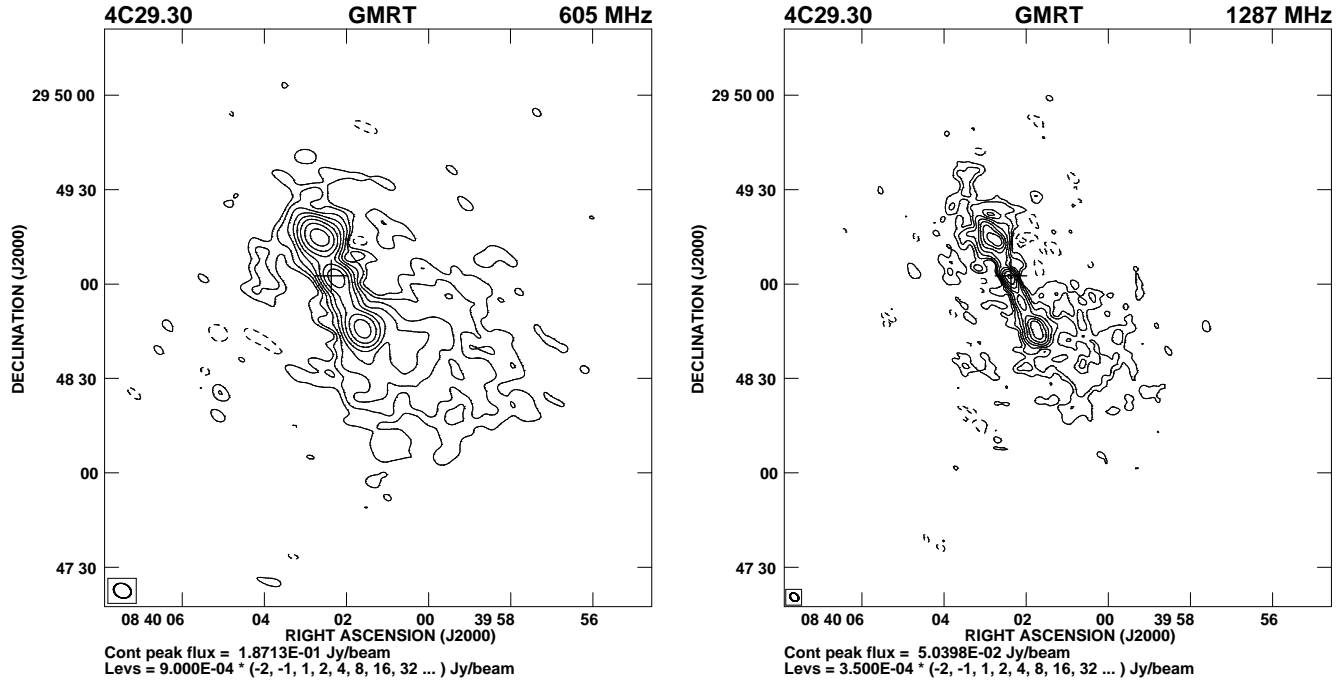


Figure 5. The GMRT images of 4C29.30. Left-hand panel: image at 605 MHz with an angular resolution of 5.66×4.50 arcsec 2 along PA 66 $^\circ$. Right-hand panel: image at 1287 MHz with an angular resolution of 2.97×2.30 arcsec 2 along PA 46 $^\circ$. The resolution is shown as an ellipse in the bottom left-hand corner while the + sign marks the position of the optical galaxy.

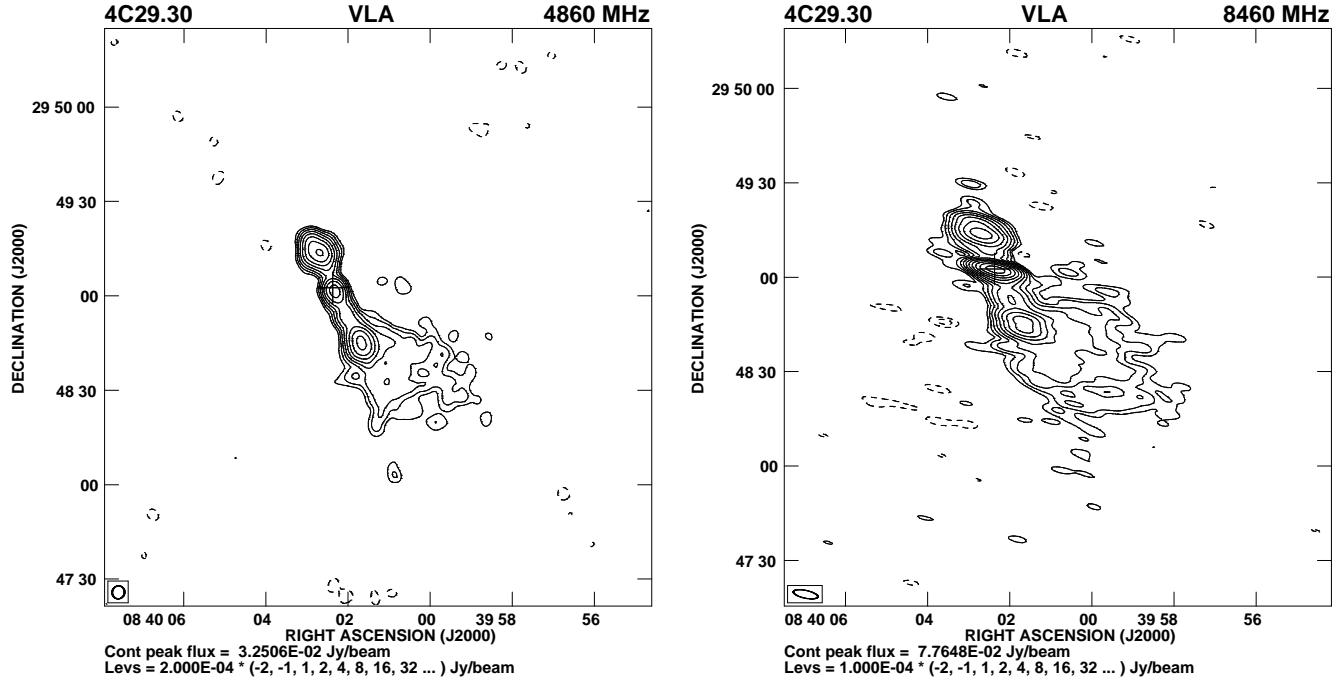


Figure 6. Left-hand panel: the VLA image of 4C29.30 at 4860 MHz with an angular resolution of 4.13×3.90 arcsec 2 along PA 162° . Right-hand panel: the VLA image at 8460 MHz with an angular resolution of 7.90×2.46 arcsec 2 along PA 78° . The resolution is shown as an ellipse in the bottom left-hand corner while the + sign marks the position of the optical galaxy.

3.2 The inner structure

The inner structure of 4C29.30 has been observed several times at different frequencies, viz. at ~ 1400 MHz (Fanti et al. 1977, van Breugel et al. 1986, Parma et al. 1986, Capetti et al. 1993), ~ 5000 MHz (Fanti et al. 1977, van Breugel et al. 1986, Giovannini et al. 1988), and ~ 15000 MHz (van Breugel et al. 1986). The maps show two arrow-shaped lobes. The more compact, northern lobe is located close to the radio core while the southern one, which is connected with the nucleus by a distinct radio jet, is more extended. The inner double-lobed structure is oriented along a PA of $\sim 26^\circ$ which is misaligned from the outer extended emission by $\sim 18^\circ$. The outer emission is oriented close to that of the optical filament towards the south noted by van Breugel et al. (1986).

The GMRT low-frequency images at 240, 333, 605 and 1287 MHz which show the inner double and the SW blob of emission are shown in Figs. 4 and 5, while the VLA images at 4860 and 8460 MHz are presented in Fig. 6. The flux densities estimated from these images are listed in Tables 2 and 3. The observational parameters and some of the observed properties are presented in Table 2, where we list the values estimated from the full-resolution images as well as those estimated from the images made by tapering and weighting the data to match the resolution of the GMRT image at 240 MHz. Table 2 is arranged as follows. Column 1: frequency of observations in MHz, with the letter G or V representing either GMRT or VLA observations; columns 2–4: the major and minor axes of the restoring beam in arcsec and its PA in degrees; column 5: the rms noise in units of mJy beam $^{-1}$; column 6: the peak flux density in the image in units of mJy

Table 2. The observational parameters and flux densities of the inner structure.

Freq. (MHz)	Beam size			rms (mJy /b)	S_p (mJy /b)	S_t^{id} (mJy)	S_t^{id+SW} (mJy)
(1)	(2)	(3)	(4)	(5)	(6)	(7)	(8)
G240	13.8	11.1	64	1.58	778	2149	2623
G333	10.6	8.5	68	1.37	527	1680	2109
	13.8	11.1	64	0.90	589	1805	2141
G605	5.66	4.50	66	0.37	187	891	1127
	13.8	11.1	64	0.24	310	1046	1196
G1287	2.97	2.30	46	0.11	50	390	490
	13.8	11.1	64	0.42	169	601	670
V4860	4.13	3.90	162	0.05	33	172	208
	13.8	11.1	64	0.13	70	208	238
V4860	16.3	4.51	65	0.10	67	242	282
V4860	14.3	4.37	72	0.22	67	242	291
V4860	14.0	4.24	71	0.09	65	242	290
V8460	7.90	2.46	78	0.03	78	188	217
	13.8	11.1	64	0.06	90	199	227

beam $^{-1}$; column 7: the total flux density of only the inner double in units of mJy; column 8: the total flux density of the inner double along with its small extension to the southwest in units of mJy. The flux densities have been estimated by specifying a polygon around the source. The error in the flux density is approximately 15 per cent at 240 MHz and 7 per cent at the higher frequencies.

Table 3. Flux densities of the radio core.

Telescope	Date of obs.	Freq.	Resn.	Flux density ^a	Refs.
(1)	(2)	(MHz)	(")	(5)	(6)
		(3)	(4)		
GMRT	2005 Dec 22	1286	~2.6	50 ^p (62 ^p)	1
VLA-B	1993 Apr 02	1400	5.4	46 ^p (46 ^p)	2
VLA-A	1982 Feb	1452	1.3	51	3
VLA-B	1982 Aug, Sep	1465	~4.0	40	4
VLA-A	1982 Feb	4873	0.3	10.4	3
VLA-A	1985 Jan	4860	~0.4	8.2	5
VLA-C	1988 Apr 14	4860	~4.0	19 ^p (21 ^p)	1
VLA-CnD	2005 Oct 9, 10	4860	~7.5	63 ^p (66 ^p)	1
VLA-CnD	2005 Oct 12	8460	~4.5	78 ^p (81 ^p)	1

^a: The core flux densities from our data and FIRST are peak values in units of mJy beam⁻¹ estimated from two-dimensional Gaussian fits to minimise contamination from extended emission. These have been marked with the superscript ^p. The remaining values are from the literature and are in units of mJy. The values within brackets are from images made with an angular resolution of 5.4 arcsec approximately along the jet axis so that the contamination from jet emission is similar. References. 1: Present paper. 2: FIRST image; 3: van Breugel et al. (1986). The flux density of C=C1+C2 in their nomenclature which would not be resolved by a ~5 arcsec beam is 16.5 mJy at 4873 MHz and 51 mJy at 1452 MHz, which is listed in the Table here. 4: Parma et al. (1986). 5: Giovannini et al. 1988. The flux density of c+A+B in their nomenclature which would be unresolved by a ~5 arcsec beam is 16 mJy.

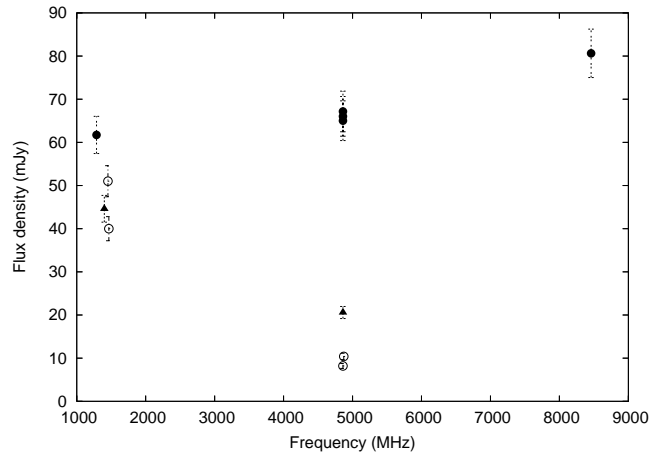


Figure 7. Spectrum of the core of 4C29.30. The measurements in 2005 with an angular resolution of 5.4 arcsec along the jet axis are shown by filled circles, while earlier observations from FIRST and our analysis of archival VLA data with a similar resolution are shown as filled triangles. The values from the literature listed in Table 3 are shown as open circles.

3.3 The radio core

Our higher-resolution images (Figs. 5 and 6) clearly show the radio core in addition to the lobes of radio emission. The J2000.0 position of the radio core estimated from our high-resolution image at 8460 MHz is RA 08^h40^m02^s.35, DEC +29°49'02".5, which is consistent with the position of the optical galaxy (RA 08^h40^m02^s.370, DEC +29°49'02".60) from

NED. van Breugel et al. (1986) and Giovannini et al. (1988) have reported observations of this source with the VLA A-array. These subarcsec-resolution images show a compact core and a radio jet towards the south-west with a prominent knot in the jet separated from the core by ~3 arcsec (3.7 kpc). With our relatively coarse resolution of a few arcsec the core flux density is contaminated by emission from the jet. From the high-resolution observations the core flux density is 10.4 mJy at 4873 MHz and 8.2 mJy at 4860 MHz (van Breugel et al. 1986; Giovannini et al. 1988), although the flux density including the knot is ~16.5 mJy.

Although our observations are of different resolutions, we have attempted to examine evidence of variability by making images with an angular resolution of 5.4 arcsec along the jet axis, which is similar to the resolution of the FIRST image, so that contamination by emission from the jet is similar at the different frequencies. A comparison of the flux densities in 2005 suggests that there was a strong outburst between about 1990 and 2005 which is apparent in the core flux densities at 4860 and also possibly at ~1300 MHz (Fig. 7). It is relevant to note that in the DDRG J1453+3308 Konar et al. (2006) reported evidence of significant variability of the core flux density at cm wavelengths. Other examples of cores which have been monitored and show evidence of variability are 3C338 and B2 1144+352 (Giovannini et al. 1998, 1999; Schoenmakers et al. 1999). It is interesting to note that both these objects are possible examples of episodic jet activity (cf. Burns, Schwendeman & White 1983; Schoenmakers et al. 1999). It is important to determine from more extensive monitoring whether strong core variability may be a common characteristic of sources with renewed jet or nuclear activity even if the cores are relatively weak. However, it is also relevant to note that strong core variability and superluminal motion may be seen in sources inclined at small angles to the line of sight. Such sources are also expected to have dominant cores due to Doppler boosting of the core flux density. Amongst the sources discussed here, the arcsec scale core in B2 1144+352 contributes almost 80 per cent of the total observed flux density at 1400 MHz, while for the other three objects it contributes \lesssim 5 per cent, similar to other galaxies of comparable luminosity (cf. Saikia & Kulkarni 1994; Ishwara-Chandra & Saikia 1999). This is consistent with the detection of superluminal motion in B2 1144+352 (Giovannini et al. 1999), while 3C338 exhibits two reasonably symmetric parsec-scale jets and evidence of subluminal motion (Giovannini et al. 1998). The cores of 4C29.30 and J1453+3308 are weak and have not been studied with mas resolution.

3.4 Spectra

The flux densities of the source, 4C29.30, from the literature as well as from our images which show the extended structure (Figs. 1, 2 and 3) are summarised in Table 4 which is self explanatory. All the flux densities are consistent with the scale of Baars et al. (1977) and where necessary have been converted to this scale using the conversion factors listed by Kühr et al. (1981). The spectrum obtained from these measurements is presented in Fig. 8 (upper panel). There are some caveats which need to be borne in mind while examining this spectrum. For the low-frequency measurements where the diffuse extended emission is more likely

Table 4. The radio flux densities of 4C 29.30.

Freq. (MHz) (1)	Flux density (mJy) (2)	Err (mJy) (3)	Ref. (4)	Note (5)
74	5393	755	1	
151	2753	147	2	
178	2220	445	3	
240	3541	496	8	(a)
325	2170	217	4	(a)
333	2647	370	8	(a)
408	1763	88	5	
605	1465	103	8	(a)
1287	727	51	8	(a)
1400	738	30	6	
1400	731	37	7	(a)
1400	756	23	8	(a)
2700	430	10	9	
4850	266	40	10	
4850	239	24	11	
4850	269	35	12	
4850	271	14	8	(a)

References along with the names of some of the well-known surveys. (1) VLSS: VLA Low-frequency Sky Survey; (2) 7C: Riley et al. 1999; (3) 4C: Pilkington & Scott 1965; (4) WENSS: Rengelink et al. 1997; (5) B2: Colla et al. 1970; (6) White & Becker 1992; (7) NVSS: Condon et al. 1998; (8) this paper; (9) Bridle et al. 1977; (10) Becker, White & Edwards 1991; (11) Langston et al. 1990; (12) Gregory & Condon 1991.

Notes: (a) The diffuse extended emission is visible in these images (Figs. 1, 2 and 3), although the entire flux density is possibly seen only in the VLA D-array image at 1400 MHz (Fig. 1) and the Effelsberg image at 4850 MHz (Fig. 2).

to make a significant contribution the noise levels are often very high and the diffuse emission may not be ‘visible’ in these observations. This can be seen clearly in the VLSS image (<http://lwa.nrl.navy.mil/VLSS>) where the rms noise is approximately 80 mJy beam⁻¹ (Fig. 9) and there is no evidence of the diffuse extended emission. The deconvolved size of this component is 64×18 arcsec² along a PA of 51°. The Cambridge 7C image of 4C29.30 at 151 MHz is towards the edge of the field and may also represent only the flux density of the inner double. The spectral index α ($\propto \nu^{-\alpha}$), determined from the total flux density of the source between 240 and 4850 MHz is 0.79 ± 0.02 .

In the lower panel of Fig. 8 we present the spectrum of the inner-double lobed source obtained from our GMRT and VLA images after subtracting the contribution of the core component at frequencies of ~ 1300 MHz and above. The total flux densities have been estimated from images which have been tapered and weighted to have the same resolution as that of the 240–MHz image. The core contribution is particularly important at 8460 MHz although it does appear to make a significant contribution at 4860 MHz. Its effect at 1400 MHz is small, its contribution being within the errors in the flux density. Our observations between 240 and 8460 MHz are consistent with a straight spectrum yielding a spectral index of 0.83 ± 0.01 for the inner double. The extrapolation of the spectrum to lower frequencies shows that the 74–MHz flux density from the VLSS is consistent with this spectral index while the Cambridge

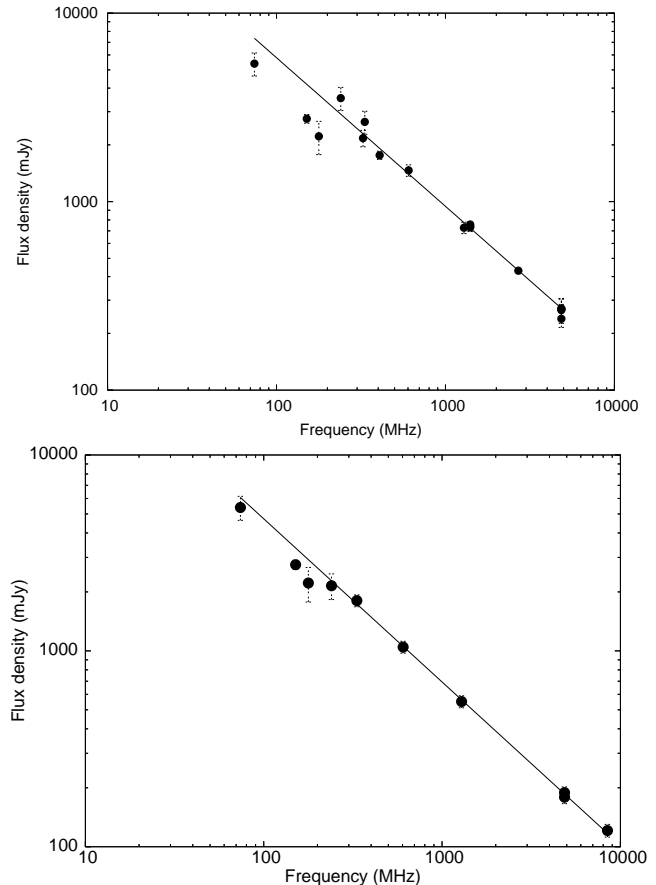


Figure 8. Upper panel: Spectrum of the 4C29.30 using the flux densities listed in Table 4. The linear least-squares fit has been made using measurements only between 240 and 4850 MHz. Lower panel: Spectrum of the inner double using our GMRT and VLA images between 240 and 8460 MHz. The contributions of the core component within a region of ~ 4 arcsec (4.9 kpc) have been subtracted at frequencies $\gtrsim 1300$ MHz. The spectrum shows the low-frequency measurements at 74, 151 and 178 MHz listed in Table 4, although the linear least squares fit has been made using measurements only between 240 and 8460 MHz. This fit has been extrapolated to lower frequencies.

measurements at 151 and 178 MHz are marginally below the expected values. We have also attempted to fit the spectrum of the inner double including the south-western blob of emission. It yields similar results with a spectral index of 0.82 ± 0.02 .

3.5 Polarization properties

The distributions of the 1400 and 4850 MHz linear polarization of 4C29.30 are shown in Fig. 10. Panels a) and c) show contours of total intensity, with E-field polarization vectors superimposed. The lengths of the vectors are proportional to the polarized intensity. Panels b) and d) show contours of polarized intensity, with E-field polarization vectors superimposed. Here, the lengths of the vectors are proportional to the fractional polarization. The integrated polarized flux densities of the central component are 41.7 ± 2.2 mJy and 7.9 ± 0.5 mJy at 1400 and 4850 MHz, respectively. The corresponding degrees of linear polarization are 6.7 ± 0.4 and

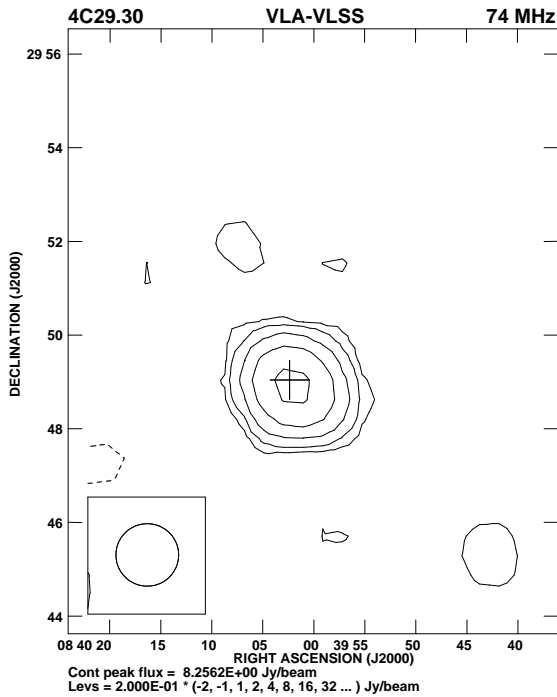


Figure 9. VLSS image of 4C29.30 with an angular resolution of 80 arcsec showing only the inner double as a single source. The resolution is shown as an ellipse in the bottom left-hand corner while the + sign marks the position of the optical galaxy.

3.3 ± 0.3 per cent. We find different orientations of the electric E-vectors in different regions of the lobes, as well as differences in the levels of polarization, suggesting Faraday rotation and depolarization effects. In order to determine the distribution of the magnetic B-field directions, it is necessary to correct the radio data for the Faraday rotation measure, and for that purpose subsequent radio polarisation measurements at other wavelengths with high angular resolution are needed. At 4850 MHz, the orientation of the E-field in the central parts of the source agrees with that reported by van Breugel et al. (1986) for the inner radio lobes (the southern one in particular). Also the large Faraday rotation measure between 5000 and 1400 MHz observed by van Breugel et al. are consistent with those indicated by our analysis. This suggests that the polarized flux is largely from the inner radio structure. However, weak linear polarization is also detected from the outer regions far beyond the inner jets and their lobes.

4 DISCUSSION

4.1 Spectral ageing analysis

The spectra using the total flux densities between 240 and 4860 MHz and that of the inner double using our measurements between 240 and 8460 MHz are consistent with a single power-law. We have fitted the spectrum of the inner double after subtracting the core flux density for the Jaffe & Perola (1973; JP), Kardashev-Pacholczyk (KP, Kardashev 1962; Pacholczyk 1970) and the continuous injection (CI,

Pacholczyk 1970) models using the SYNAGE package (Murgia 1996). The break frequency obtained from these fits are rather large ($\gtrsim 7 \times 10^5$ GHz) and have huge uncertainties because the spectrum is practically straight. These conclusions remain unaffected even if the flux density at 74 MHz is included in the analysis.

In order to calculate the global mean magnetic field strength and estimate the spectral age we have adopted the formula given by Miley (1980), a spheroidal and cylindrical geometry for the diffuse extended emission and the inner double respectively, a filling factor of ~ 1 , a proton to electron energy ratio of unity and lower- and higher-frequency cutoffs of 10 MHz and 100 GHz respectively. The equipartition magnetic field estimate for the inner double is 0.43 ± 0.06 nT, indicating that for the above-mentioned break frequency the inferred age is $\lesssim 0.12$ Myr. (For conversion of the magnetic field to μ G which is also commonly used, $1\text{nT} = 10\ \mu\text{G}$). However, adopting a more conservative break frequency of $\gtrsim 10$ GHz from the observed spectrum, the spectral age is $\lesssim 33$ Myr.

We have attempted to determine the spectrum of the diffuse extended emission by subtracting the flux density of the inner double from that of the total emission in the images where this is reliably seen. For this purpose we have used our low-resolution GMRT images at 240, 333 and 605 MHz, our VLA D-array and NVSS images at 1400 MHz and our Effelsberg measurements at 4850 MHz to represent the total flux density of the source. Our GMRT image at 333 MHz has a better rms noise than the WENSS image and gives a larger value of the total flux density. After subtracting the contribution of the inner double-lobed source, estimated from our GMRT and VLA images of similar angular resolution of ~ 12 arcsec, we plot the spectrum of the diffuse emission in Fig. 11. Although there are significant uncertainties, a least-squares fit yields a spectral index of 1.26 ± 0.07 . However, given the possibility that we are still missing significant amounts of flux density at the lower frequencies, as discussed earlier, the spectral index could be steeper. Making a very rough estimate of the possible increase in the flux density by assuming that the diffuse emission not detected at the low frequencies compared with the VLA D-array image (Fig. 1) is just below the first contour level yields a spectral index of 1.34 ± 0.05 for the diffuse emission. These points are indicated by open circles in Fig. 11. The above two values are consistent within the errors. These estimates suggest that the halo is likely to be much older than the inner double.

We have also estimated the spectral index from 240 to 1400 MHz in the vicinity of the peak in the northern diffuse emission by considering a box with a size of ~ 150 arcsec centred on the peak in the 45-arcsec resolution images. The flux densities at 240, 333, 605 and 1400 MHz are 188 ± 26 , 139 ± 19 , 87 ± 6 and 44 ± 3 mJy respectively. A least-squares fit yields a spectral index of 0.81 ± 0.01 for this region, which is similar to the spectral index of the inner double, suggesting that this value might be close to the injection spectrum, which is rather steep. The magnetic field strength in the vicinity of the peak in the northern diffuse emission is 0.12 ± 0.02 nT. The straight spectrum of this region till ~ 1400 MHz yields a spectral age of $\lesssim 100$ Myr, consistent with an interruption of activity for $\lesssim 100$ Myr. For the diffuse extended emission, the spectral break is likely to be lower

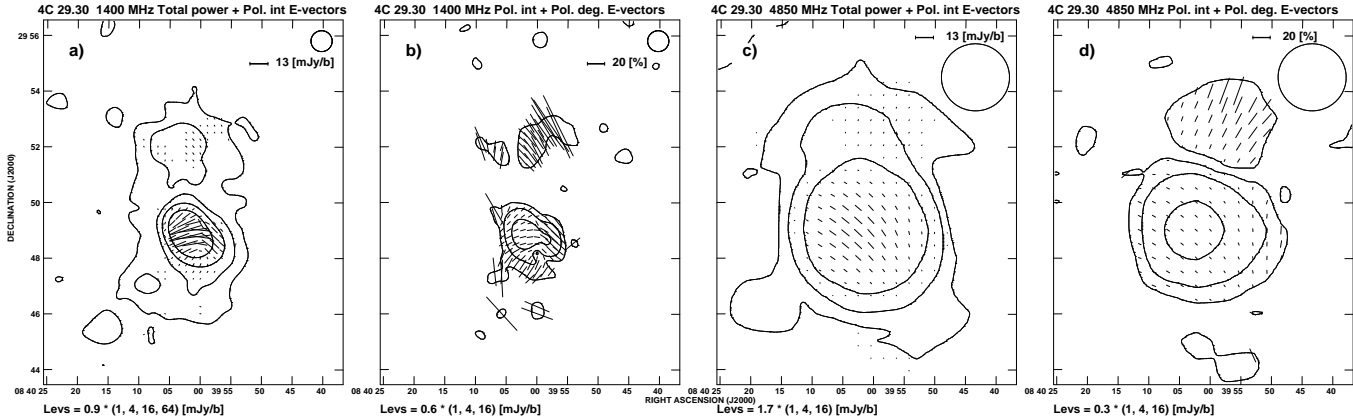


Figure 10. Polarization maps of 4C 29.30. **a)** The polarization E-vectors at 1400 MHz superimposed on the total-intensity contours and **b)** the corresponding fractional polarization vectors superimposed on the polarized intensity contours. **c)** The polarization E-vectors at 4850 MHz superimposed on the total-intensity contours and **d)** the corresponding fractional polarization vectors superimposed on the polarized intensity contours. The size of the beam is indicated by the circles in the right corners of the images and bars indicate the scale beams of the polarization vectors.

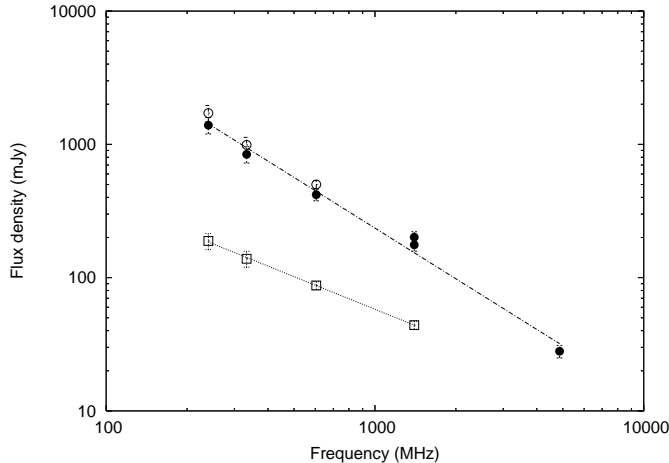


Figure 11. The radio spectrum of the diffuse emission. Filled circles denote the flux density of the diffuse extended emission after subtracting the contribution of the inner double-lobed source, the latter being estimated from our GMRT and VLA images of similar angular resolution of ~ 12 arcsec. The open circles denote the flux density after incorporating a rough estimate of the flux density not seen in the GMRT low-frequency images compared with the VLA D-array image. The open squares denote the flux densities in a box with a size of ~ 150 arcsec centred in the peak of the northern diffuse emission. The dashed lines represent the least-square fits to the points. For the diffuse emission this has been done considering only the points represented by the filled circles.

than ~ 240 MHz, which yields a spectral age $\gtrsim 200$ Myr. To get a reliable value of the spectral break and estimate the age using *SYNAGE* we need more sensitive images at low frequencies, especially below ~ 240 MHz.

Nevertheless, while interpreting these numbers caveats related to the evolution of the local magnetic field in the lobes need to be borne in mind (e.g. Rudnick, Katz-Stone & Anderson 1994; Jones, Ryu & Engel 1999; Blundell & Rawlings 2000). While Kaiser, Schoenmakers & Röttgering (2000) have suggested that spectral and dynamical ages are

comparable if bulk backflow and both radiative and adiabatic losses are taken into account in a self-consistent manner, Blundell & Rawlings (2000) suggest that this may be so only in the young sources with ages much less than 10 Myr. More recently Machalski et al. (2006) have examined the dynamical ages of FRII radio sources and find that while these agree with the spectral ages for objects less than 10 Myr, their method may be applicable for older sources as well. For all objects they find realistic jet advance velocities.

4.2 X-ray observations of the inner double

The existing Chandra data for 4C29.30 obtained on 2001 April 8 (OBSID=2135, previously analyzed by Gambill et al. 2003 and Sambruna et al. 2004) reveal x-ray emission associated with the inner radio structure. Although the photon statistics from the archival 7.5 ksec exposure is very low, several x-ray components are visible, namely a highly obscured nucleus, a diffuse galactic-scale halo, hotspot ('HS'), counter-hotspot ('C-HS'), and possibly both jets connecting hotspot and counter-hotspot with the nucleus. There is also a possible x-ray excess to the south-west from the nucleus, co-spatial with a region of enhanced optical-line emission.

We reprocessed the archival Chandra data using CALDBv.3. The 7.7-ksec ACIS-S observation detected a total of 123 ± 11 counts from the core (a circle of 1.5 arcsec radius). Most of these counts (105) exceed 2-keV energies, which indicate a very hard spectrum. The absorbed power-law model fit shows strong evidence for large intrinsic absorption of $N_H \sim (3.5 \pm 0.9) \times 10^{23} \text{ cm}^{-2}$ for the fixed photon index of $\Gamma = 1.7$, implying the intrinsic unabsorbed luminosity of $L_{2-10 \text{ keV}} \approx 3 \times 10^{43} \text{ erg s}^{-1}$. This is in agreement with the results by Gambill et al. (2003), although our number of total detected counts is larger because we used the updated Chandra calibration to process the data. Such high values of column density have been reported for some compact radio sources (e.g. Guainazzi et al. 2006; Vink et al. 2006). We note that the nucleus of 4C29.30 reveals optical features typical of Seyfert 2 and narrow-line radio galaxies (van Breugel et al. 1986).

Both hotspot and the counter-hotspot regions are pronounced in x-rays (Sambruna et al. 2004). Note that low-power radio galaxies like 4C 29.30 usually do not exhibit strong shocks at the terminal regions of the jets. The Chandra data indicate significant differences in the spectra of both features. In particular, in the case of the hotspot the number of soft (0.5 – 2 keV) and hard (2 – 10 keV) total counts is $S = 16(B=1)$, where B indicates background counts, and $H = 6(B=1)$, respectively, giving the hardness ratio $S/H = 2.9_{-1.3}^{+3.9}$; in the case of the counter-hotspots the analogous numbers are $S = 9(B=1)$, $H = 1(B=1)$, and $S/H = 10.5_{-6.5}^{+11.3}$ (see Park et al. 2006 for the description of the Bayesian methods we used to calculate the hardness ratio and errors). This suggests that the observed hotspot-related x-ray emission, especially in the counter hotspot, may be a mixture of the thermal and non-thermal radiation. The thermal scenario may be particularly relevant for the counter-hotspot region, which is in fact co-spatial with a zone of strong optical lines emission. It is interesting to note that in the radio galaxy Cen A, sharing many morphological similarities with the object discussed here, Kraft et al. (2003) reported detection of thermal x-ray emission at the counter-jet termination region due to galactic gas compressed by the expanding radio outflow. We suggest that the Chandra data may indicate similar jet/ambient medium interactions in the counter hotspot of 4C29.30, although deeper observations are needed to confirm such a scenario. In this context it is relevant to note that the line-emitting gaseous filaments extending along the inner radio structure seem to be heated and accelerated by the expanding jet rather than photoionized by the ambient medium (van Breugel et al. 1986). Evidence of similar jet-cloud interactions have been reported for many radio sources such as the compact steep-spectrum sources 3C48 (Gupta, Srianand & Saikia 2005) and 3C67, 277.1, and 303.1 (O’Dea et al. 2002).

Another interesting constraint is offered by the polarization studies. As discussed previously, the polarized flux-density from the central parts of 4C29.30 is most likely dominated by the inner lobes. As argued by van Breugel et al. (1986), large differences between the orientations of the E-vectors in this region when observed at 1400 MHz and 4850 MHz suggest Faraday rotation effects, most likely not due to the observed optical emission-line gaseous clouds, but rather due to the ‘intercloud medium’. However, similar rotation of the electric field vector is observed by us also in the outer regions, far (> 100 kpc) beyond the inner radio structure studied by van Breugel et al. This may suggest that the Faraday screen should not be identified with the gaseous medium co-spatial with the inner (\sim few kpc-scale) optical line-emitting clouds, but rather with the ambient thermal gas on larger scales, pushed-out and compressed by the expanding fossil halo, eventually partly mixed with the plasma of the lobes.

5 CONCLUDING REMARKS

We present the results of multifrequency radio observations of the radio galaxy 4C29.30 using the GMRT, the VLA and the Effelsberg telescope.

(i) The low-resolution images with the VLA, GMRT and the Effelsberg telescope show evidence of a large scale diffuse

emission with an angular scale of \sim 520 arcsec (639 kpc) in addition to the small-scale inner double which has an angular size of \sim 29 arcsec (36 kpc). The structure of the inner double is similar to that of FRII radio sources although its radio luminosity is in the FRI category. This is similar to some of the inner doubles in the DDRGs.

(ii) The GMRT and VLA observations of the inner double show that it has a spectral index of \sim 0.8 with no evidence of curvature in its spectrum from 240 to 8460 MHz, suggesting that the inner double which has an edge-brightened structure is young. We have fitted the spectrum using **SYNAGE** for the JP, KP and CI models. The break frequency is large ($\gtrsim 10^6$ GHz) but this value has huge uncertainties because the spectrum is practically straight. Its equipartition magnetic field is 0.43 ± 0.06 nT using the classical formula. The inferred spectral age for the inner double for a conservative lower limit of \sim 10 GHz for the break frequency is $\lesssim 33$ Myr.

(iii) The diffuse outer emission represents emission from an earlier cycle of activity. Its total spectrum is steep with a spectral index of \sim 1.3, with the break frequency being $\lesssim 240$ MHz. Using the classical formula the equipartition magnetic field is 0.07 ± 0.01 nT which yields a radiative age of $\gtrsim 200$ Myr.

(iv) The spectral index for the inner double as well as in the vicinity of the northern peak of the diffuse extended emission is \sim 0.8, suggesting that the injection spectral index is close to this value. Although the injection spectrum is somewhat steep, the similarity for the inner double and the outer diffuse emission is reminiscent of J1453+3308 where the outer and inner doubles have similar injection spectral indices (Konar et al. 2006).

(v) The magnetic field in the vicinity of the northern peak of the diffuse extended emission is 0.12 ± 0.02 nT. Given its straight spectrum between 240 and 1400 MHz, this yields a spectral age of $\lesssim 100$ Myr. Although higher frequency observations are required to extend the spectrum for both the inner double and the diffuse extended emission, the present data suggests a time scale of interruption of activity of $\lesssim 100$ Myr. However, the known caveats regarding estimation of spectral ages should be borne in mind.

(vi) The radio core exhibits evidence of variability. This is similar to that of the DDRG J1453+3308, suggesting that significant core variability may often occur in galaxies with evidence of recurrent activity.

(vii) The hotspots of the inner double have been detected at x-ray and optical wavelengths using the Chandra x-ray Observatory and the Hubble Space Telescope. Our reanalysis of the x-ray data suggests that the counter hotspot consists of both thermal and nonthermal material. The thermal x-ray emission may be due to hot gas compressed by the expanding radio-emitting outflow on kpc scales.

ACKNOWLEDGMENTS

We thank the anonymous referee for his valuable comments which made us re-look at our data, and present a more satisfactory interpretation of the results. We also thank Bill Cotton and Ger de Bruyn for clarifications on the VLSS and WENSS flux density scales, and Julia Riley and Dave Green for information on the 7C images and flux density scale. We thank the staffs of GMRT, VLA and the Effelsberg telescope

for their help with the observations. The GMRT is a national facility operated by the National Centre for Radio Astrophysics of the Tata Institute of Fundamental Research. The National Radio Astronomy Observatory is a facility of the National Science Foundation operated under co-operative agreement by Associated Universities Inc. The Effelsberg 100-m telescope is operated by the Max-Planck-Institut für Radioastronomie (MPIfR). This research has made use of the NASA/IPAC extragalactic database (NED) which is operated by the Jet Propulsion Laboratory, Caltech, under contract with the National Aeronautics and Space Administration. We acknowledge use of the Digitized Sky Surveys which were produced at the Space Telescope Science Institute under U.S. Government grant NAG W-2166. The images of these surveys are based on photographic data obtained using the Oschin Schmidt Telescope on Palomar Mountain and the UK Schmidt Telescope. We thank Matteo Murgia for access to the *SYNAGE* software and useful discussions. MJ was partly supported by the Polish State funds for scientific research in years 2005–2007 under contract No. 0425/PO3/2005/29. LS was supported by MEiN through the research project 1-P03D-003-29 during the years 2005–2008. This research was funded in part by NASA contract NAS8-39073: partial support for this work (AS and LS) was provided by the National Aeronautics and Space Administration through Chandra Award Number GO5-01164X and issued by the Chandra X-Ray Observatory Center, which is operated by the Smithsonian Astrophysical Observatory for and on behalf of NASA under contract NAS8-39073.

REFERENCES

Baars J.W.M., Genzel R., Pauliny-Toth I.I.K., Witzel A., 1977, *A&A*, 61, 99

Baum S.A., O'Dea C.P., de Bruyn A.G., Murphy D.W., 1990, *A&A*, 232, 19

Becker R.H., White R.L., Helfand D.J., 1995, *ApJ*, 450, 559

Becker R.H., White R.L., Edwards A.L., 1991, *ApJS*, 75, 1

Blundell K.M., Rawlings S., 2000, *AJ*, 119, 1111

Bridle A.H., Kesteven M.J.L., Brandie G.W., 1977, *AJ*, 82, 21

Burns J.O., Feigelson E.D., Schreier E.J., 1983, *ApJ*, 273, 128

Burns J.O., Schwendeman E., White R.A., 1983, *ApJ*, 271, 575

Capetti A., Morganti R., Parma P., Fanti R., 1993, *A&AS*, 99, 407

Clarke D.A., Burns J.O., Norman M.L., 1992, *ApJ*, 395, 444

Colla G., et al., 1970, *A&AS*, 1, 281

Condon J.J., Cotton W.D., Greisen E.W., Yin Q.F., Perley R.A., Taylor G.B., Broderick J.J., 1998, *AJ*, 115, 1693

Emerson D.T., Gräve R., 1988, *A&A*, 190, 353

Fanti C., Fanti R., Gioia I.M., Lari C., Parma P., Ulrich M.H., 1977, *A&A*, 61, 487

Gambill J.K., Sambruna R.M., Chartas G., Cheung C.C., Maraschi L., Tavecchio F., Urry C.M., Pesce J.E., 2003, *A&A*, 401, 505

Giovannini G., Feretti L., Gregorini L., Parma P., 1988, *A&A*, 199, 73

Giovannini G., Cotton W.D., Feretti L., Lara L., Venturi T., 1998, *ApJ*, 493, 632

Giovannini G., Taylor G.B., Arbizzani E., Bondi M., Cotton W.D., Feretti L., Lara L., Venturi T., 1999, *ApJ*, 522, 101

Gizani N.A.B., Leahy J.P., 2003, *MNRAS*, 342, 399

Gonzalez-Serrano J.I., Carballo R., Perez-Fournon I., 1993, *AJ*, 105, 1710

Gregory P.C., Condon J.J., 1991, *ApJS*, 75, 1011

Guainazzi M., Siemiginowska A., Stanghellini C., Grandi P., Piconcelli E., Azubike Ugwoke C., 2006, *A&A*, 446, 87

Gupta N., Srianand R., Saikia D.J., 2005, *MNRAS*, 361, 451

Haslam C.G.T., 1974, *A&AS*, 15, 333

Ishwara-Chandra C.H., Saikia D.J., 1999, *MNRAS*, 309, 100

Jaffe W.J., Perola G.C., 1973, *A&A*, 26, 423

Jamrozy M., Klein U., Mack K.-H., Gregorini L., Parma P., 2004, *A&A*, 427, 79

Jeyakumar S., Saikia D.J., Pramesh Rao A., Balasubramanian V., 2000, *A&A*, 362, 27

Jones D.L., Preston R.A., 2001, *AJ*, 122, 2940

Jones T.W., Ryu D., Engel A., 1999, *ApJ*, 512, 105

Junkes N., Haynes R.F., Harnett J.I., Jauncey D.L., 1993, *A&A*, 269, 29

Kaiser C.R., Cotter G., 2002, *MNRAS*, 336, 649

Kaiser C.R., Schoenmakers A.P., Röttgering H.J.A., 2000, *MNRAS*, 315, 381

Kardashev N.S., 1962, *SvA*, 6, 317

Keel W.C., Irby B.K., May A., Miley G.K., Golombek D., de Grijp M.H.K., Gallimore J.F., 2005, *ApJS*, 158, 139

Konar C., Saikia D.J., Jamrozy M., Machalski J., 2006, *MNRAS*, 372, 693

Kraft R.P., Vázquez S.E., Forman W.R., Jones C., Murray S.S., Hardcastle M.J., Worrall D.M., Churazov E., 2003, *ApJ*, 592, 129

Kronberg P.P., Reich W., 1983, *A&A*, 125, 146

Kühr H., Witzel A., Pauliny-Toth I.I.K., Nauber U., 1981, *A&AS*, 45, 367

Langston G.I., Heflin M.B., Conner S.R., Lehar J., Carrilli C.L., Burke B.F., 1990, *ApJS*, 72, 621

Lara L., Márquez I., Cotton W.D., Feretti L., Giovannini G., Mardia J.M., Venturi T., 1999, *A&A*, 348, 699

Leahy J.P., Pooley G.G., Riley J.M., 1986, *MNRAS*, 222, 753

Machalski J., Chyzy K.T., Stawarz L., Koziel D., 2007, *A&A*, 462, 43

Miley G.K., 1980, *ARA&A*, 18, 165

Morganti R., Killeen N.E.B., Ekers R.D., Oosterloo T.A., 1999, *MNRAS*, 307, 750

Murgia M., 1996, Laurea Thesis, University of Bologna

O'Dea C.P. et al., 2002, *AJ*, 123, 2333

Owen F.N., Eilek J.A., Kassim N.E., 2000, *ApJ*, 543, 611

Pacholczyk A.G., 1970, *Radio Astrophysics*, W.H. Freeman, San Francisco

Park T., Kashyap V.L., Siemiginowska A., van Dyk D.A., Zezas A., Heinke C., Wargelin B.J., 2006, *ApJ*, 652, 610

Parma P., de Ruiter H.R., Fanti C., Fanti R., 1986, *A&AS*, 64, 135

Perley R.A., Fomalont E.B., Johnston K.J., 1982, *ApJ*, 255, 93

Pilkington J.D.H., Scott P.F., 1965, *MemRAS*, 69, 183

Reich W., Stute U., Reif K., Kalberla P.M.W., Kronberg P.P., 1980, *ApJ*, 236, 61

Rengelink R.B., Tang Y., de Bruyn A.G., Miley G.K., Bremer M.N., Röttgering H.J.A., Bremer M.A.R., 1997, *A&AS*, 124, 259

Riley J.M.W., Waldram E.M., Riley J.M., 1999, *MNRAS*, 306, 31

Roettiger K., Burns J.O., Clarke D.A., Christiansen W.A., 1994, *ApJ*, 421, 23L

Rudnick L., Katz-Stone D.M., Anderson M.C., 1994, *ApJS*, 90, 955

Saikia D.J., Kulkarni V.K., 1994, *MNRAS*, 270, 897

Saikia D.J., Konar C., Kulkarni V.K., 2006, *MNRAS*, 366, 1391

Sambruna R.M., Gambill J.K., Maraschi L., Tavecchio F., Cerutti R., Cheung C.C., Urry C.M., Chartas G., 2004, *ApJ*, 608, 698

Schoenmakers A.P., de Bruyn A.G., Röttgering H.J.A., van der Laan H., 1999, *A&A*, 341, 44

Schoenmakers A.P., de Bruyn A.G., Röttgering H.J.A., van der Laan H., Kaiser C.R., 2000, *MNRAS*, 315, 371

